Urban Heat Island index based on a simplified micro scale model

Clément Marcel, Jonathan Villot

Urban Heat Island index based on a simplified micro scale model

Clément Marcel[a], Jonathan Villot[a]

[a]Mines Saint-Etienne, Univ Lyon, CNRS, UMR 5600 EVS, Institut Henri Fayol, F-42023, Saint-Etienne, France

ARTICLE INFO

ABSTRACT

The current climate changes imply the rise of the mean temperature of the cities during hot periods. To help the public policy to be more efficient about *Urban Heat Island* (UHI) reduction we aim to define a UHI risk indicator. To be useful at a local scale, the resolution of this index must be at the scale of the buildings – *i.e.* about 5 meters.

The UHI risk indicator can be mapped with the use of standard methods like direct or indirect measurements, meso or micro scale simulations, or via climate zones classifications. All these methods are not applicable over a whole territory or cannot produce map with a fine resolution as expected.

We choose here to use an intermediate approach by developing a physically based simplified micro scale model to produce a *UHI index* (ranging between 0 and 1). This model is based on data of the territory (vector data and imagery analysis) and physical laws governing heat exchanges between sun, city and atmosphere; in ideal climatic conditions (anticyclonic, without winds and clouds).

The objective is to develop an algorithm integrated into a *Geographic Information System* (GIS) software like *QGis* with a reasonable computational time to be executed on a personal computer.

1. Introduction

The current climate changes imply the rise of the mean temperatures [12][25] [12] especially into the large cities. This temperature rise increases the *Urban Heat Island* (UHI) effect that has been widely studied in the past [21] [24][22] [19] [10]. As a consequence, heat waves increase the mortality of the sensible population. Since the 2003 heat wave in Europe, many studies have focused on the risks associated with the rise of the mean temperature during summer periods [4] [8] [7].

To help the public policy to be more efficient about UHI and heat waves events we aim to define a UHI risk indicator. This indicator has to be defined at the building level to be useful at the local scale. Moreover, we aim to provide an indicator that can be assessed as fast and simple as possible to be used as a prospective point of view during urban planning stages. Lastly we focus on an indicator that can be assessed on a large territory with a personal computer.

In a previous work [3] we have studied the territory with the help of classification methods especially the *Local Climate Zone* (LCZ) classification [28]. Even if our proposed approach improves the detection of natural areas (vegetation and water) we remain blocked at a mesh cell size of about 100 meters.

In this previous work we have also applied the *World Urban Database and Access Portal Tools* (WUDAPT) methodology with the use of satellite imagery analysis [2] [1] [9]. This approach permits to have a finer level by using images with a resolution of 10 meters. On the other hand this method can be seen as a *black box* and cannot be used as a prospective way or to simulate the local effects of a particular urban planning.

---

*Corresponding author

✉ villot@emse.fr (J. Villot)

ORCID(s): 0000-0002-6568-7072 (J. Villot)

An available solution to achieve this resolution level is to use simulation of the city, by modeling and simulating the city through a meso scale or micro scale model. This method usually uses a city model under the form of an urban energy balance [11] [17]. These models are devoted to be linked with atmospheric models [15]. They are based on physical equations and produce outputs at a very fine level.

But the simulation tools come with several drawbacks:

- they require a high level of details and many data as input,

- they require a high computational effort.

Some simplified models have been developed to circumvent these problems. The literature provides some publications about simplified models [18]:

- the *Tool for Heat Island Simulation* (THIS) [20]: this model is based on the city geometry, empiric correlation from Oke [23] and some corrections done with the help of measurements,

- the *Single-Layer Urban Canopy Model linkage with a Simple Atmospheric Model* [14]: this model focuses on the comparison of the urban layer model seen as a slab model or an urban canopy model. It has been studied on an idealized case,

- the *Spatialized Urban Weather Generator* (SUWG) [16]: this model is a simplified atmospheric model that is more oriented on the simulation with weather data input,

- the *Simplified Numerical Model for Analyzing the Effects of the Urban Heat Island* [26]: this model uses a building simulation software and expects too many weather input data to be used as a simplified model.

In this paper we propose a simplified approach based on physical considerations. The objective is to maintain a high

---

level of refinement without the need of detailed description of the territory. In this way the described model has been developed starting from the available data over the territory. We aim to compute the thermal behavior of the city surfaces for a large territory on a personal computer.

The output criterion – that we have called *UHI index* – is a number between 0 and 1 that reflects the risk of UHI events locally. It is based on a physically simplified micro scale model of the city layer and a simplified atmospheric model. The objective is to provide this index with an algorithm that can be integrated into a *Geographic Information System* (SIG) like *QGis*.

2. Model presentation

The model is based on the database *BD TOPO V3* provided by *IGN* – the French agency providing geographic data of the territory. This database contains all the building footprints and heights. These data permit to construct a 3D model of the cities over the territory modeling each building as a parallelepiped. The ground is constructed as a square grid of 5 meters width without taking into account the altitude.

Building and ground surface centroids are considered as thermal nodes with dedicated thermal properties (such as inertia, albedo). We assume that the meteorologic conditions are stable (anticyclonic conditions, without winds and clouds). We choose a typical day during a heat wave from the available meteorologic data (June 27, 2019 for the station of *Saint-Etienne - Bouthéon*, (France)). We suppose that this day will repeat itself indefinitely: the simulation period is 24 hours. We choose a time-step of 1 hour.

When processing a thermal node, the surrounding surfaces are taken into account. To improve performances we limit the distance when considering surface-to-surface interactions (typically 100 meters).

2.1. Short-wave radiations

Short-wave radiations are taken into account to determine the incoming solar power over each surface. Sun is considered as a point source. For precision reasons building walls are split into many points depending on the choice of the user (by default we use one point in the horizontal direction and one point per 3 m in the vertical direction). Ray-tracing is done between surface points and sun to determine if obstruction occurs. Obstruction can be done by any rectangular vertical surface. We assume here that horizontal surfaces cannot produce any shading. These assumptions provide a simplified framework for reality description but will be sufficient to compute the incoming solar power in a fast-computing way [6].

Incoming solar heat flux is computed for each hour of the simulation period and surface albedo is applied. It should be noted that reflected light is not taken into account (energy is supposed numerically lost).

2.2. Long-wave radiations

The long-wave radiations exchanges are related to surface-to-surface and surface-to-sky exchanges. To simplify the process we suppose here that surface-to-surface exchanges are null (*i.e.* that all surrounding surfaces are at the same temperature that the processed surface). Only exchanges with the sky are taken into account here.

The *sky view factor* (SVF) is defined as the part of long-wave radiations lost from the surface to the sky over the whole radiations lost by the surface. A simplified implementation of the SVF has been proposed: N points are considered into a hemispherical surface; and ray-tracing is done between the surface centroid and any hemisphere point. For each hemisphere point i we can define:

- τ_i: the transmission ratio (a value of 1 means there is no obstruction; a value of 0 means there is an opaque obstruction), between the surface centroid and the i-th point,

- β_i: the elevation angle between the hemisphere point i and the horizontal ground (for horizontal surfaces); or the angle between the wall normal direction and the hemisphere point i (for vertical surfaces).

SVF for horizontal surfaces f_h can be approximated by the relation:

$$f_h = \frac{\pi}{2N} \sum_i \tau_i \sin \beta_i. \tag{1}$$

SVF for vertical surfaces f_v can be approximated by the relation:

$$f_v = \frac{2\pi}{5N} \sum_i \tau_i \cos \beta_i. \tag{2}$$

These relations are approximations (the numerical factors are found empirically to retrieve known values of SVF). This is because we use the definition of the SVF for an infinitesimal formulation with finite areas.

2.3. Thermal model

A thermal model is applied for each thermal node. For each node we define many properties used by the thermal model:

- thermal properties: albedo (α), specific heat (C_p), emissivity (ϵ) and convective heat exchange rate (h_c),

- structural properties: thickness (e), density (ρ), sky view factor (f), area (S).

During a time period of Δt thermal node energy amount of change can be written:

$$\Delta U = S e \rho C_p (T_{n+1} - T_n), \tag{3}$$

where T_n is the current time node temperature and T_{n+1} is the next time node temperature (after a Δt time period). The

thermal node concentrates all the mass and therefor thermal conductivity is supposed to be infinite.

We can now write all the heat exchanges applying on the thermal node during Δt. Absorbed solar energy ΔU_s can be written:

$$\Delta U_s = (1 - \alpha)P_n\Delta t \tag{4}$$

where P_n is the normal incoming direct solar energy coming to the external face of the wall, computed in a previous section.

Convective heat exchange ΔU_c can be written :

$$\Delta U_c = h_c S\Delta t(T_{a,n} - T_{n+1}), \tag{5}$$

where $T_{a,n}$ is the ambient air temperature at the current time and is given by the external conditions.

Long-wave radiations heat exchange with the sky ΔU_r can be written:

$$\Delta U_r = \sigma\epsilon Sf\Delta t(T_{s,n}^4 - T_{n+1}^4), \tag{6}$$

where $T_{s,n}$ is the deep sky temperature at the current time. For reasons of convenience we use the deep sky temperature correlation [6]:

$$T_{s,n} = \gamma T_{a,n}^{1.5}, \tag{7}$$

where γ is a numerical factor ($\gamma = 0.05532$).

The sum of all the heat exchanges (equations (4), (5) and (6)) must be equal to the internal energy variation (equation (3)).

All heat exchanges are expressed by using node temperature at the next time-step – T_{n+1} – to produce an implicit temporal scheme and avoid instabilities (or any criterion of stability).

By linearizing non-linear terms involved in (6) heat conservation equation can be rewritten:

$$A_nT_{n+1} - BT_n = C_n, \tag{8}$$

where

$$A_n = \frac{e\rho C_p}{\Delta t} + h_c + 4\sigma\epsilon f\gamma^3 T_{a,n}^{4.5}, \tag{9}$$

$$B = \frac{e\rho C_p}{\Delta t}, \tag{10}$$

$$C_n = \frac{1 - \alpha}{S}P_n + h_cT_{a,n} + 4\sigma\epsilon f\gamma^4 T_{a,n}^6. \tag{11}$$

When simulating the node for 24 time-steps (one per hour of the day) and choosing cyclic temporal boundary condition (*i.e.* $T_0 = T_{24}$) we obtain 24 equations for 24 unknown (T_0 to T_{23}):

$$\begin{aligned} A_0T_1 - BT_0 &= C_0 \\ A_1T_2 - BT_1 &= C_1 \\ &... \\ A_{22}T_{23} - BT_{22} &= C_{22} \\ A_{23}T_0 - BT_{23} &= C_{23} \end{aligned} \tag{12}$$

One can solve this system by inverting the previous linear system (12). But for optimization reasons we choose here to solve manually this system for the first temperature T_0. We can prove that

$$\begin{aligned} T_0 = \frac{1}{A_0A_1...A_{23} - B^{24}}(&C_0B^{23} + C_1A_0B^{22} \\ &+ C_2A_0A_1B^{21} \\ &+ ... \\ &+ C_{22}A_0A_1...A_{21}B \\ &+ C_{23}A_0A_1...A_{22}) \end{aligned} \tag{13}$$

Finally all other temperatures can be computed recursively with (8).

2.4. Grass covered surfaces

For modeling horizontal surfaces covered with vegetation such grass we use the previous model, and we adjust thermal properties. For this purpose [29] has been widely used. In this article the authors have performed many measures over different pavements including grass. The article provides useful data about solar power and air/grass surface temperatures. By using these data we can found that grass covered surfaces (directly exposed to sun radiation) can be modeled with these properties:

- emissivity can be considered with the value of $\epsilon = 1$,

- convective heat exchange coefficient can be set to $h_c = 67 W.m^{-2}.K^{-1}$,

- albedo can be set to $\alpha = 0.406$,

- inertia is negligible and can be set to $\rho = 0$.

Consequently, the surface covered with grass doesn't need an implicit numerical scheme resolution because of independence of temperature between two time steps. Equation (8) can be rewritten for grass cover temperature T_g:

$$T_g = \frac{(1 - \alpha)S^{-1}P + h_cT_a + 4\sigma\epsilon f\gamma^4 T_a^6}{h_c + 4\sigma\epsilon f\gamma^3 T_a^{4.5}}. \tag{14}$$

This kind of surface doesn't need temperature computation for all the time steps. Surface temperature can be computed on-the-fly when it's needed.

For mixed surfaces (*i.e.* partially covered with grass) we use the previous model without any grass coverage. When computing mean radiant temperature T_r of the surface we use the mean of impervious surface temperature T_i and surface covered with grass temperature T_g:

$$T_r = (1 - r)T_i + rT_g, \tag{15}$$

where r is the vegetation ratio of the surface (between 0 and 1). The vegetation ratio has been determined with the *Normalized difference vegetation index* (NDVI) on aerial imagery data-set with a resolution of 0.5 meter.

Figure 1: A tree and its equivalent in the model with 4 vertical rectangles (a single vertical rectangle is highlighted with red borders).

Code	Material	Category
0	undefined	Stone
1	stone	Stone
2	millstone	Stone
3	concrete	Concrete
4	brick	Brick
5	chipboard	Chipboard
6	wood	Wood
9	other	Stone

Table 1
Building wall materials defined into *MAJIC* database and corresponding categories.

2.5. Trees effects

The main trees effects are:

- shading effects from trees to vertical walls or horizontal surfaces for short-wave and long-wave incoming radiations,

- mask effects for long-wave outgoing radiations for horizontal and vertical surfaces.

Because the ray-tracing algorithm only support rectangular and vertical surfaces trees are modeled with the use of 4 vertical rectangles. The tree model must respect the following conditions:

- rectangle heights are set to tree height,

- rectangle base heights are set to 50% of the tree heights,

- the 4 rectangles are centered on the xy-plane on the tree centroid,

- the surrounding cylinder has a diameter set to the mean tree diameter (defined as the diameter of the circle that fit the tree area),

- the 4 rectangles are rotated with an angle of 45 degrees.

The figure 1 shows an example of a tree and its associated model.

Energy transmission coefficients are used when computing solar or infrared radiations. These coefficients are set to [27]:

- 20% for incoming solar radiations (short-wave and long-wave radiations),

- 50% for outgoing infrared radiations.

All the trees are grouped into a single block that act as a single transmitter element: if a vertical surface modeling a tree intersects a ray then the associated transmission coefficient is used and there is no cumulative computation done with the transmission coefficients for the other surfaces of the same block.

It should be noted that the tree effects are included in the model described here but trees are not included in the results discussed thereafter. Indeed, we have been limited by the following problems:

- first we have no information about trees in the city. Data preprocessing has provided vegetation distribution (with the use of the NDVI). We use the QGis plugin *dzetsaka* [13] to perform imagery analysis to discriminate grass and trees; but this process gives poor results in city, especially for trees that are pruned,

- second even if trees were well located we have no idea about the tree heights.

2.6. Materials assignation

The building wall materials are defined into a national database named *MAJIC*. This database assigns a code composed of 2 digits that permits to assign 0, 1 or 2 materials for each building. The materials defined into the database are shown in the table 1: the material digit code is shown in the first column ; the associated material is shown in the second one.

By studying the main material used on the territory we choose to define stone as the default material (when unknown or other materials are found). To simplify the assignation process we define many material categories - shown in the last column of the previous table. Some materials have been dropped out into a single category.

In the case where the database defines two different materials we choose to use an intermediate material (where material inertia is defined as the mean inertia of the two materials).

Standard values for material properties are used to fill in the model and are shown in the table 2.

For building roofs the default material is tile. The database materials and retained categories are shown in the table 3. The same process occurs for the assignation

Category	Albedo	Sp. heat	Density	Thick.
	−	$J.kg^{-1}.K^{-1}$	$kg.m^{-3}$	m
Stone	0.38	1000.0	2500.0	0.5
Concrete	0.20	1000.0	2300.0	0.3
Brick	0.34	1000.0	2000.0	0.2
Chipboard	0.34	1000.0	1800.0	0.2
Wood	0.40	1600.0	870.0	0.15

Table 2
Material properties for walls (Specific heat and density come from the french national thermal regulation - *RT 2012*. Albedo comes from the book *Guide solaire de l'énergie passive - Mazria - 1981*)

Code	Material	Category
0	undefined	Tile
1	tile	Tile
2	slate	Slate
3	zinc	Zinc
4	concrete	Concrete
9	other	Tile

Table 3
Building roof materials defined into *MAJIC* database and corresponding categories.

Category	Sp. heat	Density	Thickness
	$J.kg^{-1}.K^{-1}$	$kg.m^{-3}$	m
Tile	1000.0	1700.0	0.03
Slate	1000.0	2500.0	0.03
Zinc	380.0	7200.0	0.005
Concrete	1000.0	2300.0	0.2

Table 4
Material properties for roofs (Specific heat and density come from the french national thermal regulation - *RT 2012*).

of materials. The albedo is not set up by using default material values but with aerial imagery analysis [5]. The other material properties for roofs are shown in table 4.

For the materials' assignation to the ground surfaces, there is no national nor local database that provides these informations. To circumvent this lack of information we use the albedo of the ground computed with aerial imagery dataset [5].

We define three ranges of albedo to assign ground material. Thermal properties are used to define a heat penetration depth for a daily periodic signal. This depth is used to assign thickness of the material in the model. The material properties are shown in the table 5.
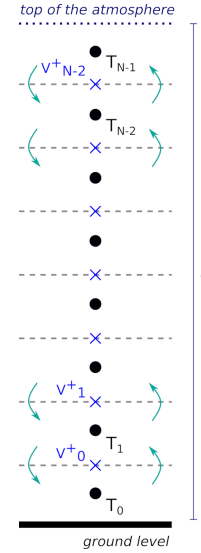
3. Atmospheric model

The atmospheric model is composed of the mesh shown in the figure 2. The atmosphere (with a height h) is split into N cells. Each cell height dh is equal to h/N.

Category	Albedo	Density	Sp. heat	Depth
	−	$kg.m^{-3}$	$J.kg^{-1}.K^{-1}$	cm
Asphalt	0.0 - 0.45	2100.0	1000.0	9.5
Granite	0.45 - 0.55	2600.0	1000.0	17.0
Marble	0.55 - 1.0	2700.0	1000.0	19.0

Table 5
Material properties for ground surfaces (Specific heat and density come from the french national thermal regulation - *RT 2012*).

Figure 2: Simplified atmospheric model.

Each cell represents an air node of volume $V = S \times dh$, where S is the ground area. The air nodes define air temperatures. In this model all pressure gradients are neglected and density is supposed constant.

On the top cell boundary we compute the mean vertical speed of the fluid (shown with a blue cross and named v_i^+ for the i-*th* air node). Assuming mass conservation during fluid movement from an air node to another, for any vertical ascending or descending flow an inverted flow must be observed. We assume that between two air nodes, mass transfer is done in an ascending way on the half of the cell area and in a descending way on the other half, as shown in figure 2.

Calling dt the time-step used for computation, ρ_a the air density, $C_{p,a}$ the air specific heat, we can write that for the i-*th* cell the energy exchange with the upper cell, dU_+ is:

$$dU_+ = \frac{1}{2}Sv_i^+ dt\rho_a C_{p,a}(T_{i+1} - T_i), \tag{16}$$

and the lower part of the energy exchange dU_- yields to:

$$dU_- = \frac{1}{2}Sv_{i-1}^+ dt\rho_a C_{p,a}(T_{i-1} - T_i). \tag{17}$$

The air node energy variation $dU = dU_+ + dU_-$ can also be written:

$$dU = Sdh\rho_a C_{p,a}(T_i^{(n+1)} - T_i^{(n)}), \tag{18}$$

where the upper-script (n) denotes the value computed at the n-*th* time-step. The equations (16) and (17) are implicitly written at the next time-step to provide an implicit temporal scheme and to avoid numerical instabilities.

These equations can be written:

$$A_i T_i^{(n+1)} = B_i T_{i+1}^{(n+1)} + C_i T_{i-1}^{(n+1)} + D T_i^{(n)}, \qquad (19)$$

where:

$$\begin{aligned}
A_i &= dh + dt(v_i^+ + v_{i-1}^+), \\
B_i &= -dt v_i^+, \\
C_i &= -dt v_{i-1}^+, \\
D &= dh.
\end{aligned} \qquad (20)$$

It should be noted that the A_i, B_i and C_i coefficients are varying during simulation: they must be computed at each time-step (with the previous values of the air speed).

3.1. Boundary conditions

There are two boundary conditions applied in the model:

- we assume that the top of the atmosphere is maintained at a fixed temperature: to apply this boundary condition we force the last temperature to be equal to the external air temperature (by forcing coefficients B_{N-1} and C_{N-1} to be null; A_{N-1} and D coefficients to be unity; and $T_{N-1}^{(n)}$ to be equal to the external air temperature for any time-step).

- heat flux injection is done on the lowest air node (*i.e.* at the ground level – the first air node is supposed to contained all the buildings). By adding the injected q power the first air node alters its equation to:

$$A_0 T_0^{(n+1)} = B_0 T_1^{(n+1)} + D T_0^{(n)} + \frac{q dt}{\rho_a C_{p,a}}. \qquad (21)$$

Injected heat flux is computed by summing all sensible heat flux released into the atmosphere:

- convective heat flux released by the building walls,

- convective heat flux released by the horizontal surfaces (roofs and ground surfaces),

- convective heat flux released by grass covered surfaces: this flux is supposed to be equal to the incoming solar power over the grass (we assume here the coarse approximation that all the incoming solar flux will be converted into sensible heat by vegetation – a more convenient hypothesis would skip latent part of the release).

Heat flux injection has been computed with surface temperatures and first air node temperature. In the thermal model these flux are computed with fixed external temperature. This weak linkage between the two models cannot assure conservatism of the energy.

It should be noted that for the first temperature there is no lower neighbor (*i.e.* C_0 coefficient is not existing); and for
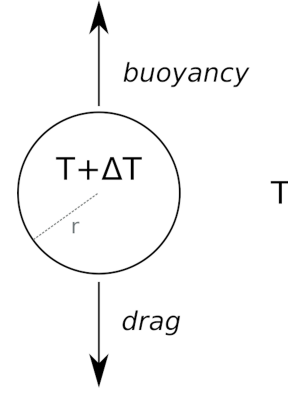

Figure 3: Fictive spherical volume of air with a radius of r.

the last temperature there is no upper neighbor (*i.e.* B_{N-1} coefficient is not existing). For these cases the A_i coefficient must be altered by removing the parts of the nonexistent coefficients.

3.2. Convective speed estimation

To estimate the vertical speed of the fluid we consider a spherical volume of air with a radius of r as depicted on the figure 3. This enclosure is located into an environment with a mean temperature of T. The air contained into the sphere has a temperature of $T + \Delta T$. We suppose here that the gas acts as a perfect gas and that the pressure variations are negligible (calling p_0 the mean pressure value).

This enclosure is subject to two forces:

- the buoyancy force f_b that will be ascending if volume is hotter than its environment (*i.e.* $\Delta T > 0$),

- the drag force f_d acting in the opposite direction to movement (opposite to the buoyancy force if inertia is neglected).

By calling Δm the mass displaced by the volume, ρ_a the air density, and g the gravity, we can write the byouancy force:

$$f_b = -g\Delta m = -g\frac{4}{3}\pi r^3 \Delta \rho_a = -g\frac{4}{3}\pi r^3 \Delta\left(\frac{p_0}{RTM_a}\right), \qquad (22)$$

where R is the perfect gas constant ($R \approx 8.314 J.mol^{-1}.K^{-1}$) and M_a is the molar mass of air ($M_a \approx 28.965 g.mol^{-1}$).

By deriving the expression in the Δ part we obtain:

$$f_b = g\frac{4}{3}\pi r^3 \frac{\Delta T p_0}{RT^2 M_a} = g\frac{4}{3}\pi r^3 \frac{p_0}{RTM_a}\frac{\Delta T}{T} = g\rho_a\frac{4}{3}\pi r^3 \frac{\Delta T}{T}. \qquad (23)$$

The drag force is classically written:

$$f_d = \frac{1}{2}C_d \rho_a S v^2, \qquad (24)$$

where $C_d = 0.5$ is the drag coefficient for a sphere; $S = \pi r^2$ is the cross-section of the sphere; and v is the mean sphere speed.

$$f_d = \frac{\pi}{4} \rho_a r^2 v^2. \tag{25}$$

At the equilibrium the 2 forces are equal and the mean vertical speed of the enclosure is given by:

$$v = \sqrt{\frac{16}{3} r g \frac{\Delta T}{T}}. \tag{26}$$

Implementation of this speed is done by considering:

- environment temperature T as the mean of the two surrounding air node temperatures,

- temperature difference ΔT as the difference of the two surrounding air node temperature.

One can write:

$$v_i^+ = \left(\frac{32}{3} r g \frac{|T_i^{(n)} - T_{i+1}^{(n)}|}{T_i^{(n)} + T_{i+1}^{(n)}} \right)^{\frac{1}{2}}. \tag{27}$$

3.3. Temperature computation

The resolution of the system is done through an iterative method to avoid using cyclic temporal boundary conditions. For the first run (*i.e.* at midnight) the vertical temperature profile is set to an initial profile (*e.g.* external air temperature). The system (which is composed of a tri-diagonal matrix) is inverted to provide all the air node temperatures. This operation is reproduced for all the day times. At the end of the day the midnight vertical profile is computed to be used as a new initial condition. The whole day is computed again until the computed midnight vertical profile differs from the previous midnight profile used as initial condition lesser than a fixed value (*e.g.* 0.1 K).

To avoid instabilities the time-step of one hour is sub-cycled (*e.g.* with a sub time-step of about 10 seconds) and iterations have been done with a relaxation factor of 0.1 for the heat flux injection.

Our model has been used with 5 vertical cells and an atmosphere height of 1000 meters. The territory has been meshed with about 74,000 horizontal cells.

3.4. Model calibration

As main drawback, the simplified atmospheric model lies on a non-physical parameter: the radius r of the fictitious volume. To calibrate the model and fix a value to this parameter we use *Computational Fluid Dynamic* (CFD) simulations. For this purpose we use the *Flowsquare+* software [30] that can solve the Euler equations for compressible fluids.

To calibrate the r value we model a unique atmosphere cell (*i.e.* a rectangular cell with a width of 100 meters and a height of 200 meters). The upper boundary imposes a cold temperature; the lower boundary imposes a hot temperature.
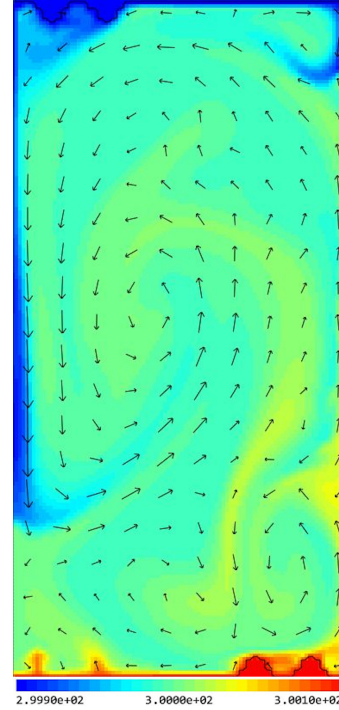

Figure 4: Atmospheric cell (100 m width; 200m height) with a vertical temperature gradient inducing air movement by buoyancy. Temperatures are between 299.9 and 300.1 K - *i.e.* a 0.2 K temperature difference. Air speeds are shown with arrows.

The buoyancy driven movements observed after many times are analyzed to extract the mean air speed.

The temperatures applied to the boundary conditions respect the condition that for any temperature difference between the two boundaries the mean temperature is set to 300 K. For example when studying the movement under a temperature difference of 5 K the boundary conditions are set to $300 \pm 2.5 K$.

The figure 4 shows the model used into Flowsquare+. We choose to compute mean air speed for a temperature difference in the range of $0 - 1$ K. The results are shown in the figure 5. Considering equation 26, $T = 300K$ and $g = 9.81 m.s^{-2}$ the best value for the r value is 0.181 meter. It should be noted that the figure 5 does not report the mean vertical ascending speed obtained by the CFD simulation (as the mean of ascending speed in the middle horizontal line). Ascending movements are not over the half area as supposed in the simplified model. The reported speed is the equivalent ascending speed if air movement was done over the half of the width of the cell.

3.5. Boundary conditions calibration

Boundary conditions are calibrated using the following procedure:

- ground level temperature varies almost like a sinusoidal curve whose amplitude only depends on the solar constant (supposed to be totally injected into the first air node): this solar constant is set up to
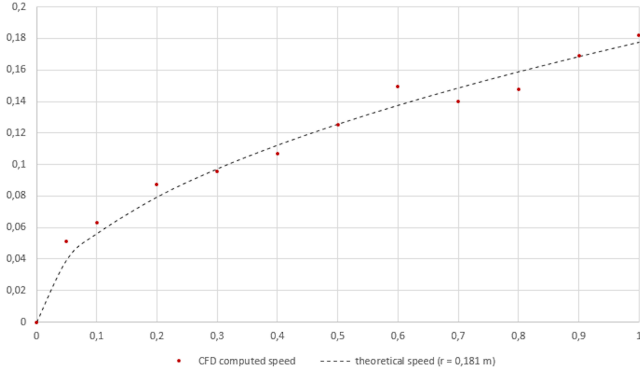
Figure 5: Mean vertical air speed (in meters per second): experimental results from CFD (red dots), theoretical speed based on a radius of 0.181 meter (dashed black line).
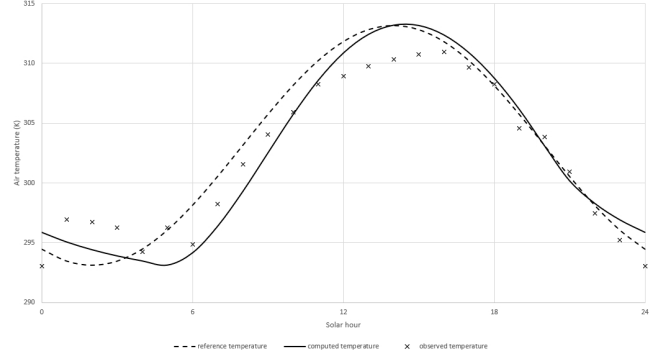

Figure 6: Ground level temperatures (in Kelvin). Meteorologic raw data (crosses) or imported as a sinusoidal curve (dashed black line) and computed temperature with the atmospheric model (solid black line).

$1316.5 W.m^{-2}$ in order to fit with the chosen typical day,

- ground level mean temperature only depends on the temperature imposed on the top of the atmosphere: this external boundary temperature is set to $290.5K$ in order to fit with the chosen typical day.

The figure 6 compares the two ground level temperature at rural location:

- the temperature computed with the simplified model (solid black line),

- the temperature of the chosen day drawn as a sinusoidal curve (dashed black line). The temperature observations used to define the sinusoidal curve are indicated with black crosses.

It should be noticed that a constant sky temperature seems to be a good assumption. Boundary temperature is defined for the chosen day for a reference altitude of 400 meters (*i.e.* the altitude of the weather station). During the simulation process this temperature is updated over the territory (using a vertical temperature gradient of 0.65 K per 100 meters).

4. UHI risk indicator

4.1. Urban felt temperature

We choose to compute the felt temperature T_f in the urban zone (excluding inner building areas) as the arithmetic mean of local air temperature T_a and radiant temperature T_r:

$$T_f = \frac{T_a + T_r}{2}. \tag{28}$$

We define the point of interest for the felt temperature in the urban area at the height of 2 meters (approximately the mean human size). Surrounding surfaces included in the mean radiant temperature are:

- the ground and roof surfaces,

- the wall surfaces.

4.2. Mean radiant temperature

The mean radiant temperature for a grid point is defined as:

$$T_r = \frac{\sum_i T_i \delta_i}{\sum_i \delta_i}, \tag{29}$$

where the subscript i stand for the i-*th* surface: T_i is surface temperature; and δ_i is defined by:

$$\delta_i = \Gamma_i \frac{S_i d_i}{r_i^3}, \tag{30}$$

where:

- Γ_i is equal to 0 if an obstruction is found between grid point and the surface, 1 otherwise,

- S_i is the surface area,

- d_i is the vertical distance between grid point and the horizontal surface or the horizontal distance between the grid point and the vertical surface,

- r_i is the distance between the grid point and the surface.

The distance between a grid point and any surface must be understood as the distance between the grid point and the surface centroid. This mean temperature is computed for surfaces that are not too far from the computed grid point (we used a default value of 20 meters).

It should be noted that the equation 30 has a bias because this expression is only applicable for infinitesimal surfaces. We use here this expression with (1) finite areas and (2) with the whole surface areas (surface can be partially masked by another surfaces).

4.3. UHI index

A common definition of the UHI is the difference of air temperature between urban and rural locations. Some observations of general trends for these differences can be noted:

- maximal air temperature difference occurs at about 09.00 PM according to Oke [24],

- minimal urban air temperature occurs at about 05.00 – 06.00 AM according to Oke [24] and confirmed by the output temperatures from the proposed model,

- maximal temperature difference seams not to overpass 10 – 12 K.

We choose here to study the UHI effects at the end of the night. This choice was guided by the fact that the trees data are not available yet. By comparing theoretical cases we show that the model has no relevant difference of temperature at the end of night if trees are taken into account or not (in the latter case trees are considered as grass).

We define the UHI index δ for each location of the map:

$$\delta = \frac{T^- - T_a^-}{\nu}, \qquad (31)$$

where T^- is the minimal felt temperature computed for the location, T_a^- is the minimal air temperature in rural conditions and ν is a normalization factor (*e.g.* $\nu = 12K$). For convenience, we impose to this index to be bounded between 0 and 1.

If one would obtain the UHI index on a coarser grid, the arithmetic mean value could be used as a good approximation.

This index can be interpreted as the local overheating in comparison with rural conditions. Due to the cyclic temporal boundary condition that acts as a hot day that repeats itself indefinitely this index will be more high when the local urban zone acts as a capacitor (capturing more sun energy and having a bad heat release coefficient).

This index convert many dynamic effects into a single static result: the overheating can be seen as the mean static effect produced by many dynamic effects (like the mean capacitor voltage produced with a variable input voltage with a null mean value). It can be seen as a local risk factor for UHI effects.

5. Results

The model has been tested over the whole territory of *Saint-Etienne Métropole* (France) which covers about 723 km² and contains 53 small or middle cities. The territory morphology is non-homogeneous with the presence of urban locations highly integrated into the surrounding nature.

The UHI index has been computed on the map with a resolution of 5 meters. About 916,000 walls and 28,000,000 horizontal surfaces have been processed during the computation. The simulation has been done on a laptop *HP ZBook 14* with *Intel Core i7-5500U* CPU and 16 Go of memory. Assigning 3 threads to perform the computation the whole process has needed about 11 hours.

The figure 7 shows an extract of the resulting map on the city center of *Saint-Etienne* (France). The map shows the
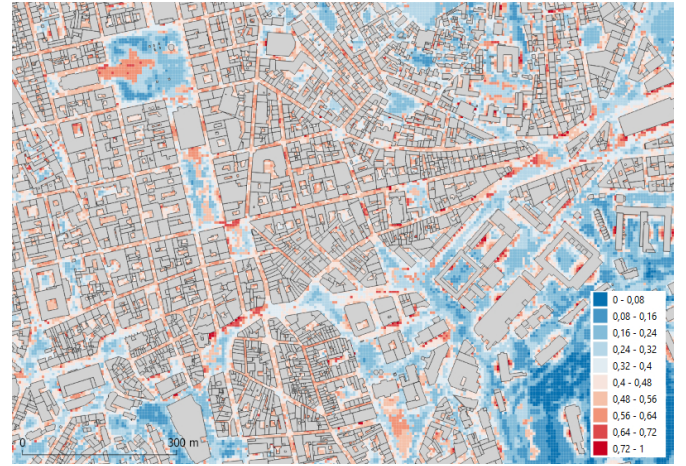

Figure 7: UHI index computed on the city center of *Saint-Etienne* (France) with a grid resolution of 5 meters.
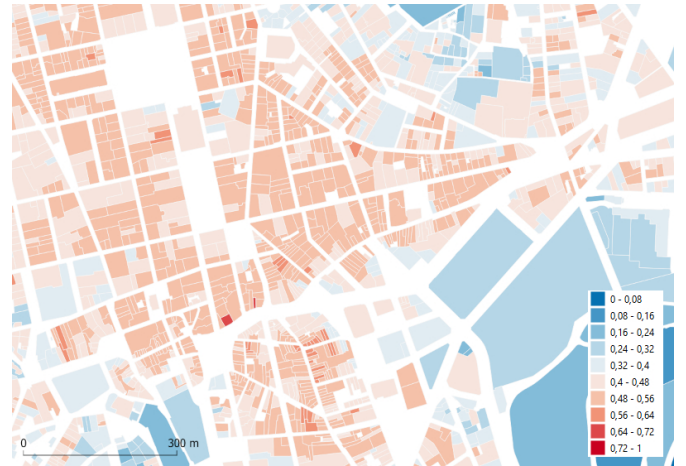

Figure 8: UHI index merged over administrative parcels, city center of *Saint-Etienne* (France).

UHI index computed over the territory with a precision of 5 meters.

The figure 8 shows the same location but with the UHI index projected over the administrative parcels. Because UHI index is only computed outside the buildings, we use the following projection method to compute UHI index on these administrative parcels: for each parcel, a buffer with a distance of 10 meters is considered, and the mean UHI index is computed in this extended area. This method provides the mean UHI index in the neighborhood of the parcel and can be representative of the direct neighborhood ambience of each building.

6. Discussion

The simplified model presented here has been successfully tested over a substantial territory on a personal computer and with a reasonable computational time. It permits to compute the UHI index on a fine grid with a resolution of 5 meters that has been imported over administrative parcels.

A validation of the model was planned by installing 30 air temperature sensors over the territory in many various points of interest. The deployment of the sensors was delayed due to the *covid19* crisis but is planned to be effective at the beginning of the year 2021.

The simplified model suffers from many approximations that can be classified from weak to strong approximations. Among all these approximations we have noted three major simplifications that can be important with respect to the precision and the quality of the results.

1. The atmospheric model assumes that all grass covered surfaces are releasing all the received solar energy under the form of sensible heat flux. No latent heat flux is taken into account but it's well known that the vegetation latent flux is the main driver used for cooling urban during overheat.

2. The linkage between the thermal model and the atmospheric model is very weak: thermal masses are releasing sensible heat flux by considering the air temperature (provided with a simple daily sinusoidal curve); the first air node computes sensible thermal flux by using its own temperature. This method doesn't ensure conservation of energy. A stronger linkage will be interesting for conservation reasons (but this strongly increases computational time).

3. The tree integration into the model has shown results that will be interesting. But the lack of information about the tree distribution and their properties (height, energy transmission, diameter, ...) will decrease the interest of the model during the day (the model has shown that the felt temperatures are the same with trees or with grass covered surfaces at the end of the night). This integration can be improved by the use of a *Digital Elevation Model* (DEM) to reconstruct the tree objects on the map.

Lastly some comparisons will be interested in the future:

1. by coupling the thermal model to an atmospheric model *e.g.* Meso-NH,
2. by comparing the results of others thermal model – *e.g. Town Energy Balance* (TEB) model with a linkage to an atmospheric model.

7. Conclusion

In this paper we have developed a simplified model based on a micro scale physical approach of the territory. The goal was to propose a QGis integration to estimate the UHI risks at the building level; that can be executed on a personal computer in a reasonable time.

The model take into account the surfaces incoming solar power; the heat exchanges with the sky; the inertia of the city buildings; the vegetation effects (grass covered surfaces and trees). The simplified atmospheric model avoid the use of CFD codes that are consuming too many computational times and is simply and weakly linked to the thermal model.

The temperature overheat at the end of the night, comparing to the rural temperature in the same conditions, has permit to define an UHI index, ranging between 0 and 1, that can be interpreted as a risk factor of overheating. This index has been defined to be computed locally – *e.g.* with a precision of 5 meters – and to be then used merged on coarser grids.

The results obtained for the territory of *Saint-Etienne Métropole* (France) has been imported into the administrative parcels, with a computational time lesser than one working day. These results will be useful to help policymakers to prevent heat waves in the future by focusing urban plannings in priority neighborhoods.

8. Funding

A. QGis integration

The simplified model has been integrated into *QGis 3.10* through a Python script. For optimization reasons computation is done into a shared library written in c language (DLL compiled for Microsoft Windows) called by the Python script.

Here are the main limitations of the implementation:

- computation is done in many threads but the DLL is nor thread-safe neither re-entrant,

- the DLL doesn't perform any kind of checks (especially for indexes that can be out of bounds),

- the solver assumes a time-step of 1 hour for a study over 24 hours with cyclic boundary conditions,

- coordinates are used as follows: x is east direction, y is north direction and z is related to elevation; all units are in meters,

- for solar power computation the solver needs to know the mean latitude of the city,

- when solving with tree obstructions, the solver assumes that the underlying coverage is grass.

References

[1] Bechtel, B., Alexander, P., Böhner, J., Ching, J., Conrad, O., Feddema, J., Mills, G., See, L., Stewart, I., 2015. Mapping local climate zones for a worldwide database of the form and function of cities. ISPRS International Journal of Geo-Information 4, 199–219. doi:10.3390/ijgi4010199.

[2] Bechtel, B., Alexander, P.J., Beck, C., Böhner, J., Brousse, O., Ching, J., Demuzere, M., Fonte, C., Gál, T., Hidalgo, J., Hoffmann, P., Middel, A., Mills, G., Ren, C., See, L., Sismanidis, P., Verdonck, M.L., Xu, G., Xu, Y., 2019. Generating wudapt level 0 data – current status of production and evaluation. Urban Climate 27, 24 – 45. URL: http://www.sciencedirect.com/science/article/pii/S221209551830302X, doi:https://doi.org/10.1016/j.uclim.2018.10.001.

[3] C., M., J., V., 2020. Mapping local climate zones with aerial imagery and territory vector data analysis. Unpublished.

[4] Canouï-Poitrine, F., Cadot, E., Spira, A., Spira, A., 2006. Excess deaths during the august 2003 heat wave in paris, france. Revue d'Épidémiologie et de Santé Publique 54, 127 – 135. URL: http://www.sciencedirect.com/science/article/pii/S0398762006767062, doi:https://doi.org/10.1016/S0398-7620(06)76706-2.

[5] Cao, C., Lee, X., Muhlhausen, J., Bonneau, L., Xu, J., 2018. Measuring Landscape Albedo Using Unmanned Aerial Vehicles. Remote Sensing 10, 1812. doi:10.3390/rs10111812.

[6] Clarke, J.A., 2001. Energy simulation in building design. Second edition ed., Butterworth-Heinemann.

[7] Conti, S., Masocco, M., Meli, P., Minelli, G., Palummeri, E., Solimini, R., Toccaceli, V., Vichi, M., 2007. General and specific mortality among the elderly during the 2003 heat wave in genoa (italy). Environmental Research 103, 267 – 274. URL: http://www.sciencedirect.com/science/article/pii/S0013935106001368, doi:https://doi.org/10.1016/j.envres.2006.06.003.

[8] D. Hémon, E.J., 2004. Surmortalité liée à la canicule d'août 2003. Technical Report. Institut National de la Santé et de la Recherche Médicale.

[9] Demuzere, M., Bechtel, B., Middel, A., Mills, G., 2019. Mapping europe into local climate zones. PLoS ONE 14, 1–27. doi:10.1371/journal.pone.0214474.

[10] Fernando, H., 2013. Handbook of Environmental Fluid Dynamics. CRC Press. doi:10.1201/b13691.

[11] Grimmond, C.S.B., Cleugh, H.A., Oke, T.R., 1991. An objective urban heat storage model and its comparison with other schemes. Atmospheric Environment. Part B 25, 311–326. doi:10.1016/0957-1272(91)90003-W.

[12] IPCC, 2019. Summary for Policymakers. In: Climate Change and Land: an IPCC special report on climate change, desertification, land degradation, sustainable land management, food security, and greenhouse gas fluxes in terrestrial ecosystems. Technical Report. Intergovernmental Panel on Climate Change.

[13] Karasiak, N., 2016. Dzetsaka qgis classification plugin. URL: https://github.com/nkarasiak/dzetsaka, doi:10.5281/zenodo.2552284.

[14] KUSAKA, H., KIMURA, F., 2004. Coupling a single-layer urban canopy model with a simple atmospheric model: Impact on urban heat island simulation for an idealized case. Journal of the Meteorological Society of Japan. Ser. II 82, 67–80. doi:10.2151/jmsj.82.67.

[15] Lafore, J.P., 1997. The Meso-NH Atmospheric Simulation System. Part I: adiabatic formulation and control simulations. Annales Geophysicae 16, 90–109. doi:10.1007/s00585-997-0090-6.

[16] Le Bras, J., Masson, V., 2015. A fast and spatialized urban weather generator for long-term urban studies at the city-scale. Frontiers in Earth Science 3, 27. URL: https://www.frontiersin.org/article/10.3389/feart.2015.00027, doi:10.3389/feart.2015.00027.

[17] Masson, V., 2000. A Physically-Based Scheme For The Urban Energy Budget In Atmospheric Models. Boundary-Layer Meteorology 94, 357–397. doi:10.1023/A:1002463829265.

[18] Mirzaei, P.A., Haghighat, F., 2010. Approaches to study urban heat island – abilities and limitations. Building and Environment 45, 2192 – 2201. URL: http://www.sciencedirect.com/science/article/pii/S0360132310001083, doi:https://doi.org/10.1016/j.buildenv.2010.04.001.

[19] Nakamura, Y., Oke, T., 1988. Wind, temperature and stability conditions in an east-west oriented urban canyon. Atmospheric Environment (1967) 22, 2691 – 2700. URL: http://www.sciencedirect.com/science/article/pii/0004698188904374, doi:https://doi.org/10.1016/0004-6981(88)90437-4.

[20] Nakata-Osaki, C.M., Souza, L.C.L., Rodrigues, D.S., 2018. This – tool for heat island simulation: A gis extension model to calculate urban heat island intensity based on urban geometry. Computers, Environment and Urban Systems 67, 157 – 168. URL: http://www.sciencedirect.com/science/article/pii/S0198971516301053, doi:https://doi.org/10.1016/j.compenvurbsys.2017.09.007.

[21] Nunez, M., Oke, T.R., 1977. The Energy Balance of an Urban Canyon. Journal of Applied Meteorology 16, 11–19. doi:10.1175/1520-0450(1977)016<0011:TEBOAU>2.0.CO;2.

[22] Oke, T., 1988. Street design and urban canopy layer climate. Energy and Buildings 11, 103 – 113. doi:10.1016/0378-7788(88)90026-6.

[23] Oke, T.R., 1981. Canyon geometry and the nocturnal urban heat island: Comparison of scale model and field observations. Journal of Climatology 1, 237–254. URL: https://rmets.onlinelibrary.wiley.com/doi/abs/10.1002/joc.3370010304, doi:10.1002/joc.3370010304, arXiv:https://rmets.onlinelibrary.wiley.com/doi/pdf/10.1002/joc.3370010304.

[24] Oke, T.R., 1982. The energetic basis of the urban heat island. Quarterly Journal of the Royal Meteorological Society 108, 1–24. doi:10.1002/qj.49710845502.

[25] Oke, T.R., Mills, G., Christen, A., Voogt, J.A., 2017. Urban Climates. Cambridge University Press. doi:10.1017/9781139016476.

[26] Oropeza-Perez, I., 2020. Simplified numerical model for analyzing the effects of the urban heat island upon low-rise buildings by using a free-license thermal simulation program. Urban Science 4. URL: https://www.mdpi.com/2413-8851/4/2/30, doi:10.3390/urbansci4020030.

[27] Shahidan, M., Jones, P., 2008. 179: Plant canopy design in modifying urban thermalenvironment: Theory and guidelines.

[28] Stewart, I.D., Oke, T.R., 2012. Local Climate Zones for Urban Temperature Studies. Bulletin of the American Meteorological Society 93, 1879–1900. doi:10.1175/BAMS-D-11-00019.1.

[29] Takebayashi, H., Moriyama, M., 2012. Study on surface heat budget of various pavements for urban heat island mitigation. Advances in Materials Science and Engineering 2012, 1–11. URL: https://doi.org/10.1155/2012/523051, doi:10.1155/2012/523051.

[30] Yuki Minamoto, H.C., 2018 (accessed September 23, 2020). Flowsquare+. URL: https://fsp.norasci.com/en/.